Cell. Mol. Life Sci. 66 (2009) 1570 – 1579
1420-682X/09/091570-10
DOI 10.1007/s00018-009-9065-y

Cellular and Molecular Life Sciences

Research Article

Structure/function analysis of a critical disulfide bond in the active site of L-xylulose reductase

H.-T. Zhao[a, †], S. Endo[b, †], S. Ishikura[b], R. Chung[a], P. J. Hogg[c], A. Hara[b] and O. El-Kabbani[a, *]

[a] Medicinal Chemistry and Drug Action, Monash Institute of Pharmaceutical Sciences, 381 Royal Parade, Parkville, Victoria 3052 (Australia), Fax: 61-3-9903-9582, e-mail: ossama.el-kabbani@pharm.monash.edu.au
[b] Laboratory of Biochemistry, Gifu Pharmaceutical University, Mitahora-higashi, Gifu 502 – 8585 (Japan)
[c] UNSW Cancer Research Centre, University of New South Wales, Sydney, New South Wales 2052 and Children's Cancer Institute Australia for Medical Research, Randwick, New South Wales 2031 (Australia)

Received 25 January 2009; received after revision 12 February 2009; accepted 16 February 2009
Online First 2 April 2009

Abstract. L-Xylulose reductase (XR) is involved in water re-absorption and cellular osmoregulation. The crystal structure of human XR complemented with site-directed mutagenesis (Cys138Ala) indicated that the disulfide bond in the active site between Cys138 and Cys150 is unstable and may affect the reactivity of the enzyme. The effects of reducing agents on the activities of the wild-type and mutant enzymes indicated the reversibility of disulfide-bond formation, which resulted in three-fold decrease in catalytic efficiency. Furthermore, the addition of cysteine (>2 mM) inactivated human XR and was accompanied by a 10-fold decrease in catalytic efficiency. TOF-MS analysis of the inactivated enzyme showed the S-cysteinylation of Cys138 in the wild-type and Cys150 in the mutant enzymes. Thus, the action of human XR may be regulated by cellular redox conditions through reversible disulfide-bond formation and by S-cysteinylation.

Keywords. L-xylulose reductase, short-chain dehydrogenase/reductase, X-ray crystallography, site-directed mutagenesis, disulfide bond, protein structure, enzyme regulation.

Introduction

L-Xylulose reductase (XR; EC 1.1.1.10) belongs to a group of enzymes comprising the glucuronic acid/uronate cycle of glucose metabolism which accounts for approximately 5 % of the total glucose catabolized per day [1]. The enzyme catalyses the NADPH-linked reduction of L-xylulose to xylitol as well as that of several types of pentoses, tetroses and trioses [2, 3]. Since XR also efficiently reduces various α-dicarbonyl compounds including endogenous diacetyl, it is called dicarbonyl/L-xylulose reductase and is identical to diacetyl reductase (EC 1.1.1.5). The enzyme is highly expressed in liver and kidney of the human and has been shown to be localized in the brush-border membranes of proximal tubular cells of the mouse kidney, suggesting a role for the enzyme in water re-absorption and cellular osmoregulation by producing xylitol [3]. Moreover, enzymes of the glucuronic acid pathway are present in mammalian lens, and the flux of sugars and xylitol through this pathway has been suggested to be involved in the osmoregulation process of the lens and the etiology of sugar cataracts [4]. In apoptosis of human T lymphoma cells induced by 9,10-phenanthrenequinone, a major component in

† These two authors contribute equally to this work.
* Corresponding author.

diesel exhaust particles, XR is upregulated and deteriorates the apoptotic signaling through the generation of reactive oxygen species [5]. Recently, XR was identified as a biomarker for prostate cancer [6] and may contribute to melanoma progression [7]. Therefore, the determination of the structure-function relationship for the enzyme may lead to the development of specific inhibitors of XR to be used as potential anti-cancer agents.

XR is composed of 26 kDa subunits, each consisting of 244 amino acids, and is a member of the short-chain dehydrogenase/reductase (SDR) superfamily [2, 3, 8]. The crystal structure of human XR has been determined as a dimer and more recently the quaternary structure of the physiological tetramer was reported [9, 10]. The residues comprising the proposed catalytic tetrad in the SDR enzymes are conserved in human XR (Asn107, Ser136, Tyr149, and Lys153) and although the role of Asn107 in the coenzyme binding is more important for human XR, its additional role in substrate binding was also suggested [10]. The crystal structures showed a disulfide bond between Cys138 and Cys150, present within the active site pocket. Disulfide bonds were reported earlier to serve two main functions: influencing the thermodynamics of protein folding, as well as maintaining protein structural integrity [11, 12]. However, recent reviews suggested that the function of some proteins/receptors is controlled by cleavage of one or more of their disulfide bonds, as the cleavage is mediated by catalysts or facilitators that are specific for the substrate protein [13, 14].

We describe a crystal structure of the dimeric form of human XR with one monomeric unit that has the side-chain of Cys138 near the substrate-binding site exhibiting a double conformation; an oxidized conformer where a disulfide bond existed between Cys138 and Cys150 and was accompanied by the binding of a phosphate ion in the active site, and a reduced conformer where no disulfide bond was present. In the other monomeric unit, only the reduced conformer was present and the side-chain of Cys138 formed a covalent bond with an hydroxide ion. We demonstrate the reversibility of the disulfide formation between Cys138 and Cys150 by incubating human XR in the presence or absence of the reducing agents 2-mercaptoethanol (2ME), dithiothreitol (DTT) and glutathione (GSH), as well as the kinetic effects of the disulfide formation. Furthermore, we investigate the role of Cys138 in the enzyme reaction by analyzing kinetic alteration induced by S-cysteinylation of Cys138 in XR and site-directed mutagenesis of Cys138Ala.

Materials and methods

Materials. High purity reagents and coenzymes were obtained from Sigma-Aldrich Chemical Company. Crystallization kits were initially obtained from Hampton Research.

Site-directed mutagenesis, expression, and purification. Mutation of Cys138Ala was introduced into the cDNA for human XR in an expression vector [3] using a QuickChange site-directed mutagenesis kit (Stratagene) and a set of forward and reverse primers (30 base pairs) containing the desired mutated Ala codon (GCC), as described previously [15]. The PCR product was inserted at the restriction sites of the pRset vector (Invitrogen), and the coding regions were sequenced by using a CEQ2000XL DNA sequencer (Beckman Coulter) to confirm the presence of the desired mutation and to ensure that no other mutation had occurred. The mutant and wild-type XRs were expressed in *Escherichia coli* BL21 (DE3) and purified to homogeneity from the cell extracts using buffers containing 2 mM 2ME as previously described [3].

Crystallization. The wild-type human XR (18 mg/mL) in buffer A (10 mM Tris-HCl, pH 7.5, containing 2 mM 2ME and 20 % glycerol) was subjected to buffer replacement with buffer B (10 mM Tris-HCl, pH 7.5, containing 2 mM 2ME) prior to crystallization. This was carried out in a 0.5 mL-microcon centrifugal unit (Millipore) using a Biofuge "Fresco" centrifuge (Heraeus) set at 7300 x g by repeated cycles of concentration and dilution with buffer B. Following buffer replacement, the enzyme was brought to a concentration of 17.2 mg/mL for crystallization trials. These experiments were carried out at 22 °C in a 24-well tissue culture plate *via* the vapor diffusion method [16]. Before crystallization, 66 μL of XR (17.2 mg/mL) in buffer B was mixed with 1 μL of NADPH (84.2 mM) to yield a molar ratio of 1 : 8. Each droplet consisted of 2 μL of enzyme-NADPH mixture mixed with 0.4 μL of xylitol (to a final concentration of 20 % w/v) and 1.6 μL of solution from the well (15 % PEG 8000, 0.05 M potassium phosphate and 0.1 M MES buffer, pH 6.5). Crystals grew within one week to an average dimension of 0.30 × 0.30 × 0.34 mm.

Data collection and analysis. X-ray diffraction data was recorded at -173 °C from an XR crystal using a MAR345 image plate mounted on a Rigaku RU-300 rotating-anode X-ray generator operated at 50 kV and 90 mA. Each frame was recorded with a 600 s exposure and a 1° oscillation around ϕ. The crystal to detector distance was set to 150 mm so that the

Table 1. Data collection and refinement statistics (values in the parentheses are for the outer resolution shell).

Data collection		
	Space group	$P2_12_12$
	Unit cell dimensions	$a = 73.68$ Å $b = 87.48$ Å $c = 72.17$ Å
	No. molecules in asymmetric unit	2
	Resolution range (Å)	30–1.87 (1.94–1.87)
	Total no. of reflections	190201 (19651)
	Unique reflections	37468 (3363)
	R_{sym} (%)	6.3 (33.9)
	Completeness (%)	98.1 (95.7)
	Redundancy	5.0 (5.6)
	Mean I/σ (I)	12.6 (2.5)
Refinement statistics		
	Resolution limits (Å)	30–1.87
	R_{free}	0.258 (0.343)
	R_{work}	0.204 (0.357)
	No. non-H protein atoms	4321
	No. of NADPH molecules	2
	No. of Phosphate molecules	1 (50% occupancy)
	No. water molecules	557
	Mean B factors (Å^2)	
	Protein atoms	28
	NADPH	32.9
	Phosphate	50.6
	Waters	39.3
	RMS deviations from ideal geometry	
	Bond distances (Å)	0.022
	Bond angles (°)	1.9
	Dihedral angles (°)	23.3
	Ramachandran statisitics	
	Most favored (%)	90.3
	Favored (%)	9.7

$R_{sym} = \Sigma|(I_{hkl}) - I_{hkl}|/|I_{hkl}|$, where (I_{hkl}) is the average intensity over symmetry-related reflections and I_{hkl} is the observed intensity. $R_{value} = \Sigma||F_o| - |F_c||/\Sigma|F_o|$, where F_o and F_c are the observed and calculated structure factors. For R_{free} the sum is done on the test set reflections (5% of total reflections), for R_{work} on the remaining reflections.

spots were well resolved. The data were processed and scaled using the *HKL* software package [17]. Data collection and processing statistics are shown in Table 1. Assuming that two molecules (MW of 26500 Da) are present in the asymmetric unit, the Matthews coefficient (V_M) was calculated as 2.24 Å^3 Da^{-1}, and the estimated solvent content was 45.1%.

Structure determination and refinement. The structure of human XR in space group $P2_12_12$ was determined with the molecular replacement method using the atomic coordinates of the binary XR complex (PDB code: 1PR9), where only the oxidized form of the Cys138-Cys150 disulfide bond was observed, as the search model and the program *MOLREP* from the *CCP4* suite of programs [18]. The conformations of the amino acid side chains were determined from Fourier maps (*2Fo-Fc and Fo-Fc*), the structure was refined using *REFMAC5* from *CCP4*, water molecules were added using the molecular-graphics program *COOT* [19], and the models were examined using the program *XtalView* [20]. Data collection and refinement statistics for the structure are given in Table 1. Coordinates and structure factor

amplitudes have been deposited in the protein data bank (PDB 3D3W) and will be immediately released upon publication.

Analysis of the disulfide bond between Cys138-Cys150. The structural features of the Cys138-Cys150 disulfide bond for each monomer of the human L-xylulose reductase structure with the oxidized Cys residues (PDB 1PR9; [10]) were determined as described previously [21, 22]. The disulfide bond analysis tool is available at http://www.cancerresearch.unsw.edu.au/CRCWeb.nsf/page/Disulfide+Bond+Analysis.

The secondary structures in which the Cys reside and their solvent accessibility values are from DSSP (http://swift.cmbi.ru.nl/gv/dssp/). The dihedral strain energy of the disulfides was estimated from the magnitude of the five χ angles that constitute the bond [21, 23, 24]. This calculation does not include factors such as bond lengths, bond angles, and van der Waals contacts, but it has been shown to provide semi-quantitative insights into the amount of strain in a disulfide bond [25–28]. The configuration of the disulfide bonds was classified according to the sign of the five χ angles [21, 22].

Enzyme activity measurement. The reductase activities of the wild-type and Cys138Ala mutant XRs were assayed by measuring the change of NADPH absorbance (at 340 nm) in a 2.0 mL reaction mixture, which consisted of 0.1 M potassium phosphate, pH 7.0, 0.1 mM NADPH, 5.0 mM diacetyl and enzyme. One unit of enzyme activity is the amount of enzyme which catalyzes the oxidation of 1 μmol of NADPH per min at 25 °C.

Modification by thiol compounds. The enzyme solutions (40 μg/mL in 10 mM potassium phosphate buffer, pH 7.0) were incubated in the absence or presence of the thiol compounds at 25 °C. An aliquot (25 μL) of the solution was taken for assaying the remaining activity. In the identification of the modified residues of human wild-type and Cys138Ala mutant XRs by Cys, the enzyme solutions (0.1 mg/mL in the phosphate buffer containing 0.5 mM 2ME) were incubated with 10 mM Cys for 1 h at 25 °C, and the buffer was replaced with 10 mM potassium phosphate buffer, pH 7.0 as described above. The enzyme samples were denatured by adding acetonitrile (50%), and digested by trypsin (2.5 μg/mL) for 12 h at 25 °C. The tryptic digest was analyzed using a Mass Spectrometry System Ultraflex TOF/TOF (Bruker-Franzen, Bremen, Germany) with a saturated α-cyano-4-hydroxy cinnamic acid matrix. Protein identification using the peptide mass fingerprint data was performed by the MASCOT search engine (http://www.matrixscience.com) against the amino acid sequence of untreated wild-type and Cys138Ala mutant XRs.

Results

Structure of XR. The structure of human XR was refined to a resolution of 1.87 Å. The space group is $P2_12_12$ with unit cell parameters $a = 73.68$ Å, $b = 87.48$ Å, $c = 72.17$ Å, $\alpha = \beta = \gamma = 90.0^\circ$. There were two XR molecules per asymmetric unit, with the molecules forming the dimer designated as A and B each consisting of 244 amino acid residues plus 557 water molecules in the final structure. Electron density corresponding to a bound xylitol in the crystal structure was not observed. The final R_{work} and R_{free} values were 0.204 and 0.258, respectively. A total of 90.3% of the residues in the XR structure were within the most favoured region and 9.7% in the allowed region of the Ramachandran plot [29]. The estimated mean coordinate error from the Luzatti plot analysis was 0.2169 Å [30]. The final refinement statistics are summarized in Table 1. All 244 amino acid residues of the two subunits of the enzyme were fitted into corresponding electron density and, as observed in the previously determined 1.96 Å resolution crystal structure of human XR [10], each subunit is a single protein domain with a "α/β doubly wound" structure consisting of a central seven-stranded parallel β-sheet surrounded by arrays of three α helices. Two shorter helices are located away from the main domain body and constitute parts of the substrate-binding cleft (Fig. 1). The binding conformation of the NADPH molecule was described in the 1.96 Å resolution crystal structure of human XR [10]. However, unlike the published structure, the current refinement showed that the side-chain of Cys138 existed in a double conformation in one of the two XR molecules and in the reduced form in the second molecule.

As shown in Figure 2A, in the first conformation the side chain of Cys138 of molecule A, present near the substrate-binding site formed a disulfide bond with Cys150 and a phosphate ion, used as the crystallization salt, was adjacently bound. In the second conformation there was no disulfide bond present between Cys138 and Cys150, as these residues were present in their reduced forms. Due to the orientation of the sulfhydryl group of Cys138, the phosphate ion bound in the active site observed in the oxidized conformer was not present. Only the reduced form of Cys138 was present in molecule B of the dimer, shown in Figure 2B, and, similarly, due to the orientation of the sulfhydryl group of Cys138, there was no phosphate

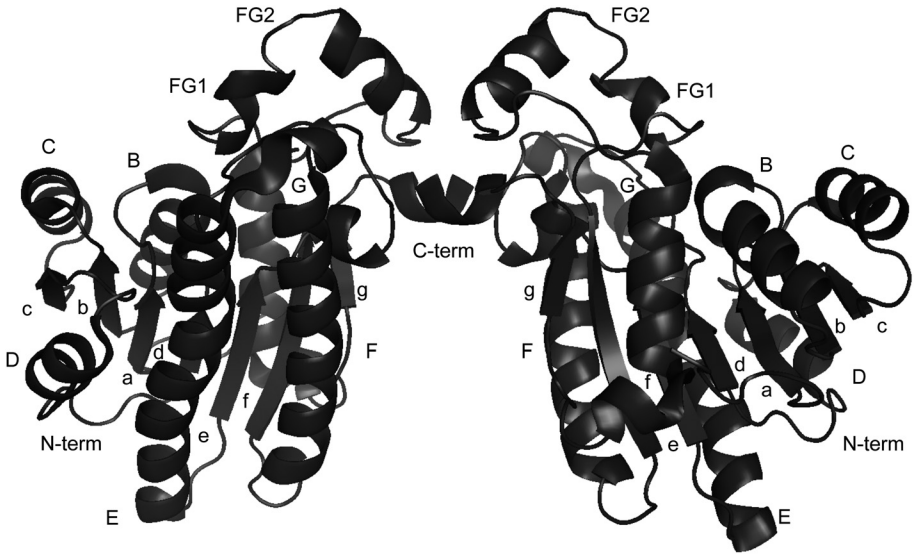

Figure 1. The human XR dimer. The α-helices are indicated by capital letters *B*–*G*, FG1, and FG2. The β-sheets are labeled in lower case letters a–g. The α-helices, FG1 and FG2, are the only regions protruding away from the main body of the subunits. Figure was prepared using MOLSCRIPT [37].

ion bound in the active site. However, in this case the side chain of Cys138 formed a sulfanol group through a covalent bond with a hydroxide ion.

In the published crystal structure of the XR holoenzyme [10] the Cys138-Cys150 disulfide links a 3/10 helix (Cys138) and an α-helix (Cys150) (Table 2). The disulfide bond in both molecules of the dimer has a –/+ left-handed hook (–/+LHHook) configuration and a high average dihedral strain energy of 43 kJ.mol^{-1}. For comparison, the mean strain energy of a dataset of 6874 unique disulfide bonds in X-ray structures is 15 kJ.mol^{-1} [21]. There were 254 –/+LHHook's in this dataset with a mean dihedral strain energy of 16 kJ.mol^{-1}. The estimated strain energy of the Cys138-Cys150 disulfide, therefore, is almost three times the average strain energy of all disulfides in published X-ray structures. This high strain energy is expected to render the disulfide bond more susceptible to reduction [25–28].

Both Cys of the disulfide bond are exposed to solvent to some extent. The averaged DSSP scores of the dimer for solvent accessibility are 8 and 18 for Cys138 and Cys150, respectively (Table 2). The surface exposure of the disulfide bond is consistent with its possible manipulation by endogenous oxidoreductases.

Effects of depletion and addition of thiol compounds on the activity of wild-type human XR. When the purified enzyme containing 2 mM 2ME was diluted with 10 mM potassium phosphate, pH 7.0, so that the concentration of 2ME was 12.5 μM, its diacetyl reductase activity was gradually decreased (Fig. 3). The decrease in activity was completely prevented by

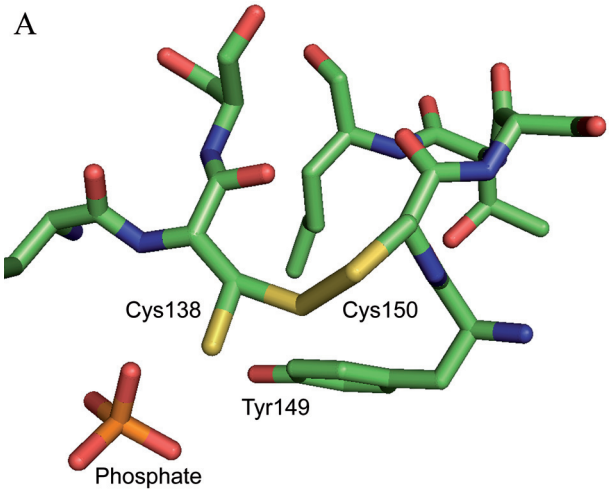

Figure 2. Close-up view showing the area of Cys138 and Cys150 for each molecule (*A* and *B*) of the XR dimer. Figures were prepared using PyMOL [38].

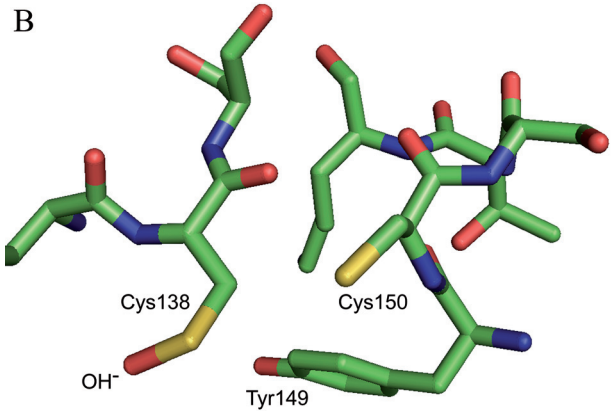

Figure 2. *(continued)*

Table 2. Features of the Cys138-Cys150 disulfide bond in human XR (PDB 1PR9).

Cys138 Chain	Cys138 Secondary structure[#]	Cys138 Solvent accessibility[#]	Cys150 Chain	Cys150 Secondary structure[#]	Cys150 Solvent accessibility[#]	Dihedral Energy* (kJ.mol^{-1})	Configuration
A	3/10 helix	9	A	α helix	18	44.5	–/+LHHook
B	3/10 helix	7	B	α helix	18	41.9	–/+LHHook

[#] Secondary structures and solvent accessibility of the Cys residues are from DSSP (http://swift.cmbi.ru.nl/gv/dssp/)
* The dihedral strain energy of the disulfides was estimated as described previously [21, 23, 24].

Table 3. Summary of the kinetic constants of human wild-type (WT) and Cys138Ala mutant XRs with or without various treatments. The untreated enzymes were diluted with 10 mM potassium phosphate buffer containing 2 mM 2ME, and the other enzyme samples were treated as shown in arrows in Figures 3, 4A, and 5A.

Enzyme	K_m (μM)	V_{max} (units/mg)	V_{max}/K_m (units/mg/mM)
Untreated WT	94 ± 5	8.7 ± 0.3	93
WT oxidized by incubation with buffer alone, (a) in Figure 3	150 ± 8	4.3 ± 0.2	30
WT reactivated by treatment with 2ME, (b) in Figure 3	90 ± 2	8.7 ± 0.3	96
WT reactivated by treatment with DTT, (c) in Figure 3	88 ± 6	8.5 ± 0.1	96
WT inactivated by treatment with Cys, (*) in Figure 4A	220 ± 20	2.6 ± 0.1	12
Untreated Cys138Ala	220 ±10	29 ± 2	134
Cys138Ala inactivated by incubation with Cys, (*) in Figure 5A	410 ± 10	6.5 ± 0.2	16

the addition of 2 mM 2ME and DTT, and partially by that of 2 mM GSH. It should be noted that more than 0.4 mM concentrations of 2ME were needed to protect against the loss of enzyme activity. The loss of the activity induced by removing 2ME was rapidly recovered by the addition of 2 mM 2ME and DTT, although such effect of GSH was not significant.

The enzyme that was incubated for 60 min in the buffer alone (a in Fig. 3) showed 1.6-fold higher K_m for the substrate and 2-fold lower V_{max} than those of the untreated enzyme (Table 3). The treatment of the inactivated enzyme with 2ME and DTT (b and c, respectively, in Fig. 3) recovered not only activity but also kinetic properties where the K_m and V_{max} values were almost the same as those of the 2ME-diluted enzyme. Based on the present crystal structure, these results indicate that the purified XR exists in the reduced (SH) form, the disulfide bond between Cys138 and Cys150 is formed only by removing 2ME from the enzyme solution, and the formed disulfide bond is easily reduced by the addition of 2ME and DTT.

In contrast to the preventive effects of 2ME, DTT, and GSH against disulfide formation, the incubation of the reduced (SH) form of XR in the presence of Cys caused a significant and progressive inactivation of the enzyme. Both the rate and maximal extent of inactivation were dependent on the Cys concentration (Fig. 4A). The inactivation was not complete as approximately 20% of the activity remained after incubation for 1 h with 10 mM Cys. The activity of the Cys-inactivated enzyme was not recovered by the addition of 10 mM DTT and 2ME (data not shown). The modification by Cys resulted in a 2-fold increase in K_m value as well as a 3-fold decrease in the V_{max} value compared with the untreated SH-form of the

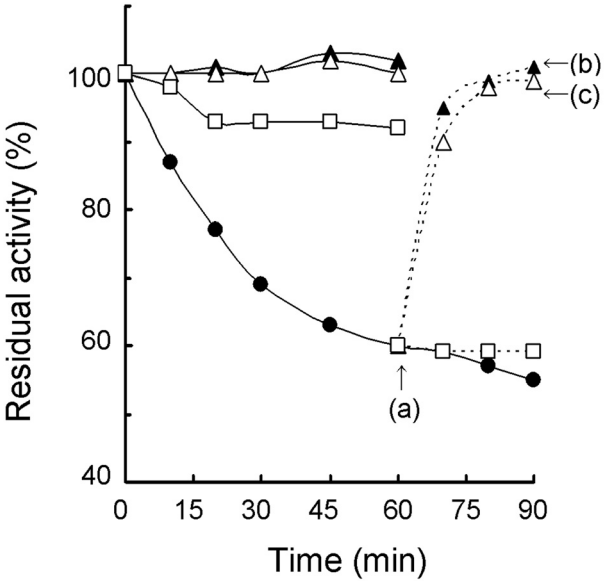

Figure 3. Effects of reducing agents on inactivation of human XR diluted with 10 mM potassium phosphate, pH 7.0. The enzyme was diluted to 40 μg/mL with the phosphate buffer (●) or the buffers containing 2 mM 2ME (▲), 2 mM DTT (Δ) and 2 mM GSH (□), and then the residual activity was assayed at indicated times of the incubation at 25 °C. At 60 min after incubation of the enzyme diluted with the buffer alone (shown by an arrow, a), 2 mM 2ME (▲), 2 mM DTT (Δ) and 2 mM GSH (□) were added (dashed lines). The enzyme samples obtained at arrows (a), (b) and (c) were used for kinetic analysis in Table 3.

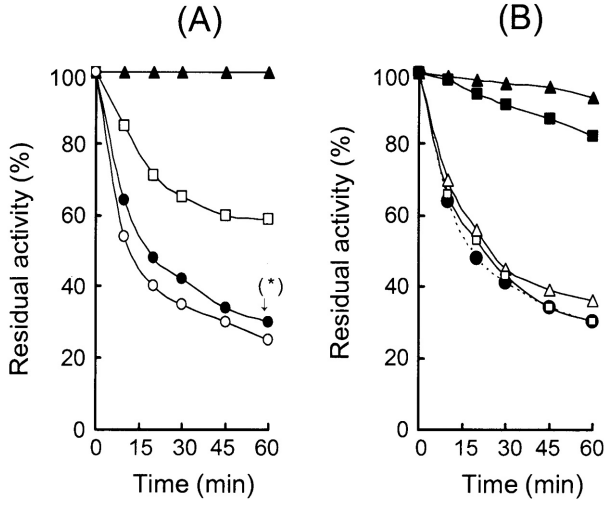

Figure 4. (*A*) Inactivation of human XR by Cys. The SH-form enzyme solution (40 μg/mL in 10 mM potassium phosphate, pH 7.0, containing 0.5 mM 2ME) was incubated at 25 °C without (▲) or with 2 mM (□), 5 mM (●) and 10 mM (○) Cys, and the residual activity was measured. The enzyme sample obtained at an arrow (*) was used for kinetic analysis in Table 3. (*B*) Effects of NADP(H) and *n*-butyric acid on Cys-induced inactivation of the SH form XR. The enzymes were incubated at 25 °C in the presence of 5 mM Cys and the following compounds: none (●, dashed line), 1 mM $NADP^+$ (□), 1 mM NADPH (Δ), 1 mM $NADP^+$ plus 0.5 mM *n*-butyrate (■) or 1 mM NADPH plus 0.5 mM *n*-butyrate (▲).

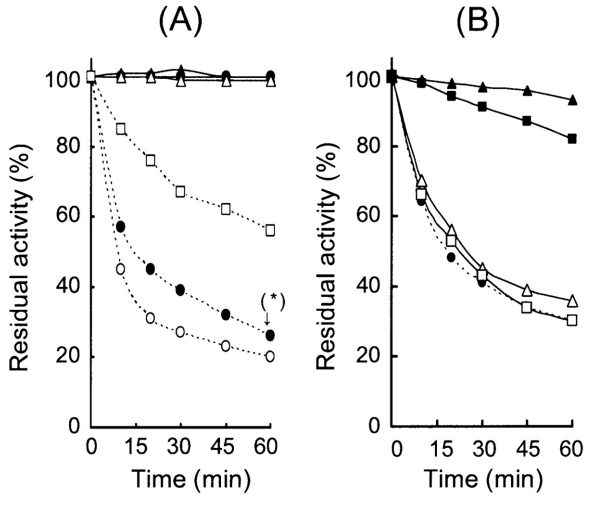

Figure 5. (*A*) Effects of thiol compounds on the activity of Cys138A mutant XR. The enzyme solution (40 μg/mL in 10 mM potassium phosphate, pH 7.0) was incubated at 25 °C without (●) or with 2 mM 2ME (▲), 2 mM DTT (Δ), or Cys (dashed lines), and the residual activity was measured. The concentrations of Cys: 2 mM (□), 5 mM (●) and 10 mM (○). The enzyme sample obtained at an arrow (*) was used for kinetic analysis in Table 3. (*B*) Effects of NADP(H) and *n*-butyric acid on Cys-induced inactivation of the mutant enzyme. The enzymes were incubated at 25 °C in the presence of 5 mM Cys and the following compounds: none (●, dashed line), 1 mM $NADP^+$ (□), 1 mM NADPH (Δ), 1 mM $NADP^+$ plus 0.5 mM *n*-butyrate (■) or 1 mM NADPH plus 0.5 mM *n*-butyrate (▲).

enzyme (Table 3). The Cys-induced inactivation was prevented by the addition of both NADP(H) and a competitive inhibitor, *n*-butyric acid [3], but not by the addition of the coenzyme alone (Fig. 4B), suggesting that the residue(s) in the active site of the enzyme is (are) modified by the added Cys.

Cys138Ala mutant XR. Unlike wild-type XR, the mutant enzyme was stable in the phosphate buffer and its activity was not influenced by 2ME and DTT (Fig. 5A), supporting the disulfide formation between Cys138 and Cys150 in the purified wild-type enzyme by the removal of 2ME from the enzyme solution. In contrast, Cys inactivated the Cys138Ala mutant, and the time- and dose-dependent effects were almost the same as those of the wild-type SH-form of XR. In addition, like the case of the wild-type enzyme, the activity of the Cys-inactivated mutant enzyme was not recovered by the addition of 10 mM DTT and 2ME (data not shown), and the inactivation was prevented by the addition of both NADP(H) and competitive inhibitor, *n*-butyric acid, but not by the addition of the coenzyme alone (Fig. 5B). Furthermore, the K_m for diacetyl and V_{max} values were elevated and decreased, respectively, by incubation with 5 mM Cys, and the extent of the kinetic alteration was similar to that of the disulfide formation of the wild-type enzyme by removing 2ME (Table 3).

S-Cysteinylation of XR. The inactivation of both wild-type and Cys138Ala mutant XRs by Cys suggested a possibility that Cys residue(s) is (are) covalently modified by the addition of Cys. To identify the modified residues, we examined the tryptic peptides derived from the enzymes treated with 10 mM Cys for 1 h by matrix-assisted laser desorption/ionization time-of-flight mass spectrometry (MALDI-TOF-MS). We determined the sequences (composed of a total 117 residues) of nine tryptic peptides derived from the two Cys-inactivated enzymes, of which only two peptide fragments, Gly126–Arg141 and Ala142–-Lys153, contain Cys138 and Cys150, respectively. In the wild-type XR, the m/z value of the Gly126–Arg141 fragment was 1720.9, which was larger by 120 mass than the value of 1600.8 of the corresponding fragment derived from the untreated enzyme. The difference of the values corresponded to one Cys molecule, and was actually observed in the Cys138 residue. In contrast, the Ala142–Lys153 fragment showed the same m/z value of 1309.5 as the corresponding fragment derived from the untreated enzyme, implying that Cys150 was not modified. Thus, the result indicated that at least Cys138 is S-cysteinylated by the incubation of wild-type XR. Among the analyzed peptides derived from the Cys-inactivated mutant enzyme, the Ala142–Lys153 fragment showed the

larger m/z value of 1428.7 than the value (1309.5) of the corresponding peptide derived from the untreated mutant enzyme, implying that Cys150 was S-cysteinylated in the mutant enzyme. No increase in the m/z value was observed in other peptides, including the Gly126–Arg141 fragment that has Ala138 in this mutant enzyme. The sequences (m/z values) determined for seven other peptides were fMet1–Arg9 (1092.5), Gly22–Arg33 (1181.6), Glu98–Arg109 (1482.6), Ala110–Arg120 (1183.6), Val162–Lys171 (1094.5), Ile172–Lys196 (2739.2) and Thr199–Lys208 (1142.6), which were the same in all analyzed enzymes.

Discussion

Since the determination of the first crystal structure of human XR binary complex the involvement of the disulfide bond present in the active site pocket of the enzyme between Cys138 and Cys150 in the regulation of enzyme activity has not validated by other methods [9, 10]. However, as shown in Figure 2, the refinement of the present structure did not show electron density corresponding to a disulfide bond between Cys138 and Cys150 in molecule B of the dimer, where the side-chain of Cys138 formed a covalent bond with a hydroxide. A double conformation was observed in molecule A where one conformer of Cys138 formed a disulfide bond with Cys150 in the oxidized form, along with the presence of a phosphate ion bound in the active site, and the second conformer was present in the reduced form. A close analysis of the nature of the disulfide bond suggested that it may be present in the enzyme as a means to regulate the activity rather than just to maintain the overall structure. Based on geometrical analysis, the disulfide bond conformation was classified as a –/+LHHook, a conformation associated with an unusually high dihedral strain energy, and hence can be easily broken for regulation of enzyme activity [21].

The progressive loss of enzyme activity by the removal of 2ME and its complete recovery by the addition of 2ME and DTT (Fig. 2) suggested that, first, Cys138 and Cys150 exist as the free SH forms in the purified wild-type XR, and secondly, the formed disulfide bond between the two residues was structurally unstable. This is supported by the kinetic alterations by these treatments, and is in good agreement with the new crystal structure of human XR and geometrical analysis of the S-S bond, indicating that this bond is highly strained and hence may be easily broken for the regulation of the enzyme activity. Compared with 2ME and DTT, GSH showed a low protective effect against the formation of the S-S bond and apparently no reduction of the formed S-S bond. Since GSH, a tripeptide, is relatively larger than 2ME and DTT, its access to, and influence on Cys138 and/or Cys150 in and near the active site of the enzyme may be less pronounced. The formation of the S-S bond decreased the catalytic efficiency for diacetyl reduction to one-third of that of the reduced SH form of XR. Thus, the catalytic action of human XR may be influenced by cellular redox conditions through the reversible formation of the S-S bond, although the physiological significance of this phenomenon remains unknown at present.

While Cys150 is conserved in mammalian XRs, Cys138 of human XR is replaced with alanine [2, 3]. Human XR shows lower K_m and k_{cat} (i.e. V_{max}) values than other animal XRs. The mutation of Cys138Ala resulted in a 2 – 3 fold increase in the kinetic constants for diacetyl, although the values are still low compared to those of other animal XRs. Previous crystal structures of binary complexes of human XR showed that Cys138 is one of the substrate-binding residues [9, 10]. The kinetic alteration by Cys138Ala demonstrated that this residue participates in the binding of diacetyl, and also suggested that the residue difference at this position is one reason for the kinetic difference between human and other animal XRs. The role of Cys138 in substrate binding is also supported by more significant impairment of the kinetic alteration resulting from the cysteinylation of Cys138 of wild-type XR that was demonstrated by the MALDI-TOF/MS analysis. Although Cys150 has not been described as a substrate-binding residue in previous crystallographic studies of human XR [9, 10], a similar extent of the kinetic alteration was observed by cysteinylation of Cys150 of the Cys138Ala mutant. In the present crystal structure of the enzyme, the side-chain of Cys150 is located close to the catalytic residue Tyr149 (Fig. 2B) and the substrate-binding residue Val143. The additional Cys residue moiety on the cysteinylated Cys150 may affect the orientation of these two residues in the substrate-binding pocket, thus influencing both the binding of the substrate and the dissociation of the product.

Human XR contains five Cys residues, two of which (Cys138 and Cys150) are located close to the catalytic pocket. The results of the MALDI-TOF/MS reveal that at least Cys138 in the wild-type enzyme and Cys150 in the Cys138Ala mutant were thiolated by the added Cys, although we can not rule out the possibility that other Cys residues are modified. The modification of the two Cys residues is also supported by the alteration of the kinetic constants due to the cysteinylation and prevention of the Cys-induced inactivation by the coenzyme plus competitive inhibitor, but not by the coenzyme alone. In the wild-type enzyme the presence of the reduced side-chain of Cys138

within the substrate-binding pocket (Fig. 2B) makes it the preferred candidate for the selective modification by the added Cys, and once Cys138 is modified it sterically prevents the modification of Cys150, which is located further away from the binding pocket. In the case of the Cys138Ala mutant, due to the relatively small methyl side-chain compared to CH_2-SH of the wild-type, there is sufficient space that allows the added Cys to reach and modify the side-chain of Cys150.

Recently, S-cysteinylation has been reported for bacterial proteins [31] and mammalian proteins, such as albumin [32], MHC class II ligands [33], protein kinase C [34] and aldose reductase [35]. In most of these reports, cystine, and not Cys, was predicted or demonstrated to act as a direct protein thiolator. In contrast, Cys itself reacts with Cys138 or Cys150 in the case of human XR and its mutant as described above. Cys, like 2ME and DTT, is a small molecule that might bind in the catalytic pocket of XR, modifying the Cys residues. In addition, the cysteinylation of human XR is irreversible because the enzyme activity was not restored by the addition of 2ME or DTT, that lead to the release of the modified Cys moiety from other cysteinylated proteins [33 – 35]. Since the irreversible S-cysteinylation by Cys resulted in a large decrease in catalytic efficiency of human XR, it will be important to demonstrate the S-cysteinylation of the enzyme in cellular models and investigate its physiological significance.

The newly-determined human XR structure indicated that the disulfide bond between Cys138 and Cys150 could be broken, and results obtained from disulfide bond analysis as well as site-directed mutagenesis along with kinetic studies, have shown that the disulfide bond may affect the reactivity of the enzyme. Recently, there has been a report of an intra-subunit disulfide bond located in 3β-hydroxysteroid dehydrogenase, a member of the SDR family, which enhances the affinity of the enzyme for substrates and cofactors [36]. Similarly, the importance of the disulfide bond in regulating the activity of human XR, another member of the SDR family, has been demonstrated in this study. Due to recent evidence implicating XR with the development of cancer [6, 7], enhanced understanding of the function of the disulfide bond present in the active site of human XR may lead to the discovery of new inhibitors to be used as lead compounds in the development of new anti-cancer agents.

1 Hollmann S., and Touster O. (1964). Metabolism of glucuronic and ascorbic acids. In: Non-glycolytic pathways of metabolism of glucose. (New York: Academic Press), pp. 107–113.
2 Ishikura, S., Isaji, T., Usami, N., Kitahara, K., Nakagawa, J., and Hara, A. (2001). Molecular cloning, expression and tissue distribution of hamster diacetyl reductase. Identity with L-xylulose reductase. Chem. Biol. Interact. 130–132, 879–889.
3 Nakagawa, J., Ishikura, S., Asami, J., Isaji, T., Usami, N., Hara, A., Sakurai, T., Tsuritani, N., Oda, K., Takahashi, M., Yashimoto, M., Otsuka, N., and Kitamura, K. (2002). Molecular characterization of mammalian dicarbonyl/L-xylulose reductase and its localization in kidney. J. Biol. Chem. 277, 17883–17891.
4 Goode, D., Lewis, E., and Crabbe, J. (1996). Accumulation of xylitol in the mammalian lens is related to glucuronate metabolism. FEBS Lett. 395, 174–178.
5 Matsunaga, T., Kamiya, T., Sumi, D., Kumagai, Y., Kalyanaraman, B., and Hara, A. (2008). L-xylulose reductase is involved in 9,10-phenanthrenequinone-induced apoptosis in human T lymphoma cells. Free radical biology & medicine, 44, 1191–1202.
6 Cho-Vega, J. H., Tsavachidis, S., Do, K. A., Nakagawa, J., Medeiros, L. J., and McDonnell, T. J. (2007). Dicarbonyl/L-xylulose reductase: a potential biomarker identified by laser-capture microdissection-micro serial analysis of gene expression of human prostate adenocarcinoma. Cancer Epidemiol. Biomarkers Prev. 16, 2615–2622.
7 Cho-Vega, J. H., Vega, F., Schwartz, M. R., and Prieto, V. G. (2007). Expression of dicarbonyl/L-xylulose reductase (DCXR) in human skin and melanocytic lesions: morphological studies supporting cell adhesion function of DCXR. J. Cutan. Pathol. 34, 535–542.
8 Jörnvall, H., Danielsson, O., Hjelmqvist, L., Persson, B., and Shafqat, J. (1995). The alcohol dehydrogenase system. Adv. Exp. Med. Biol. 372, 281–294.
9 El-Kabbani, O., Carbone, V., Darmanin, C., Ishikura, S., and Hara, A. (2005). Structure of the tetrameric form of human L-xylulose reductase: probing the inhibitor-binding site with molecular modeling and site-directed mutagenesis. Proteins 60, 424–432.
10 El-Kabbani, O., Ishikura, S., Darmanin, C., Carbone, V., Chung, R., Usami, N., and Hara, A. (2004) Crystal structure of human L-xylulose reductase holoenzyme: probing the role of Asn 107 with site-directed mutagenesis. Proteins 55, 724–732.
11 Thornton, M. (1981). Disulphide bridges in globular proteins. J. Mol. Biol. 151, 261–287.
12 Wetzel, R. (1987). Harnessing disulfide bonds using protein engineering. Trends Biochem. Sci. 12, 478–482.
13 Hogg, P. J. (2003). Disulfide bonds as switches for protein function. Trends Biochem. Sci. 28, 210–214.
14 Chen, M., and Hogg, P. J. (2006). Allosteric disulfide bonds in thrombosis and thrombolysis. J. Thromb. Haemost. 4, 2533–2541.
15 Ishikura, S., Isaji, T., Usami, N., Nakagawa, J., El-Kabbani, O., and Hara, A. (2003). Identification of amino acid residues involved in substrate recognition of L-xylulose reductase by site-directed mutagenesis. Chem. Biol. Interact. 143–144, 543–550.
16 McPherson, A. (1985). Crystallization of macromolecules: general principles. Methods Enzymol. 114, 112–120.
17 Otwinowski, Z., and Minor, W. (1997). Processing of X-ray diffraction data collected in oscillation mode. Methods Enzymol. 276, 307–326.
18 Collaborative Computational Project, Number 4. (1994). The CCP4 suite: programs for protein crystallography. Acta Crystallogr. D 50, 760–763.
19 Emsley, P., and Cowtan, K. (2004). Coot: model-building tools for molecular graphics. Acta Crystallogr. D 60, 2126–2132.
20 McRee, E. (1999). XtalView/Xfit – a versatile program for manipulating atomic coordinates and electron density. J. Struct. Biol. 125, 156–165.
21 Schmidt, B., Ho, L., and Hogg, P. J. (2006). Allosteric disulfide bonds. Biochemistry, 45, 7429–7433.
22 Schmidt, B., and Hogg, P. J. (2007). Search for allosteric disulfide bonds in NMR structures. BMC Struct. Biol. 7, 49.

23 Katz, B. A., and Kossiakoff, A. (1986). The crystallographically determined structures of atypical strained disulfides engineered into subtilisin. J. Biol. Chem. 261, 15480–15485.
24 Weiner, S. J., Kollman, P. A., Case, D. A., Singh, U. C., Ghio, C., Alagona, G., Profeta, S. J., and Weiner, P. (1984). A new force field for molecular mechanical simulation of nucleic acids and proteins. J. Am. Chem. Soc. 106, 765–784.
25 Kuwajima, K., Ikeguchi, M., Sugawara, T., Hiraoka, Y., and Sugai, S. (1990). Kinetics of disulfide bond reduction in alpha-lactalbumin by dithiothreitol and molecular basis of super-reactivity of the Cys6-Cys120 disulfide bond. Biochemistry (Mosc) 29, 8240–8249.
26 Pjura, P. E., Matsumura, M., Wozniak, J. A., and Matthews, B. W. (1990). Structure of a thermostable disulfide-bridge mutant of phage T4 lysozyme shows that an engineered cross-link in a flexible region does not increase the rigidity of the folded protein. Biochemistry (Mosc) 29, 2592–2598.
27 Wells, J. A., and Powers, D. B. (1986). In vivo formation and stability of engineered disulfide bonds in subtilisin. J. Biol. Chem. 261, 6564–6570.
28 Wetzel, R., Perry, L. J., Baase, W. A., and Becktel, W. J. (1988). Disulfide bonds and thermal stability in T4 lysozyme. Proc. Natl. Acad. Sci. USA 85, 401–405.
29 Ramakrishnan, C., and Ramachandran, G. (1965). Stereochemical criteria for polypeptide and protein chain conformations. II. Allowed conformations for a pair of peptide units. Biophys. J. 5, 909–933.
30 Luzzatti, V. (1952). Traitement Statistique des Erreurs dans la Determination des Structures Cristallines. Acta Crystallogr. 5, 802–810.
31 Hochgräfe, F., Mostertz, J., Pöther, D. C., Becher, D., Helmann, J. D., and Hecker, M. (2007). S-cysteinylation is a general mechanism for thiol protection of *Bacillus subtilis* proteins after oxidative stress. J. Biol. Chem. 282, 25981–25985.
32 Bar-Or, D., Heyborne, K. D., Bar-Or, R., Rael, L. T., Winkler, J. V., and Navot, D. (2005). Cysteinylation of maternal plasma albumin and its association with intrauterine growth restriction. Prenat. Diagn. 25, 245–249.
33 Haque, M. A., Hawes, J. W., and Blum, J. S. (2001). Cysteinylation of MHC class II ligands: peptide endocytosis and reduction within APC influences T cell recognition. J. Immunol. 166, 4543–4551.
34 Chu, F., Ward, N. E. and O'Brian, C. A. (2003). PKC isozyme S-cysteinylation by cystine stimulates the pro-apoptotic isozyme PKCδ and inactivates the oncogenic isozyme PKCε. Carcinogenesis 24, 317–325.
35 Vilardo, P. G., Scaloni, A., Amodeo, P., Barsotti, C., Cecconi, I., Cappiello, M., Lopez Mendez, B., Rullo, R., Dal Monte, M., Del Corso, A., and Mura, U. (2001). Thiol/disulfide interconversion in bovine lens aldose reductase induced by intermediates of glutathione turnover. Biochemistry 40, 11985–11994.
36 Thomas, J. L., Huether, R., Mack, V. L., Scaccia, L. A., Stoner, R. C., and Duax, W. L. (2007). Structure/function of human type 1 3β-hydroxysteroid dehydrogenase: An intrasubunit disulfide bond in the Rossmann-fold domain and a Cys residue in the active site are critical for substrate and coenzyme utilization. J. Steroid Biochem. Mol. Biol. 107, 80–87.
37 Kraulis, P. (1991). MOLSCRIPT: a program to produce both detailed and schematic plots of protein structures. J. Appl. Crystallogr. 24, 946–950.
38 DeLano, L. (2002). The PyMOL Molecular Graphics System. DeLano Scientific, San Carlos. CA, USA. http://www.pymol.org.